Neutron diffraction study on structural and magnetic properties of La₂NiO₄

J Rodríguez-Carvajal, M T Fernández-Díaz and J L Martínez

Institut Laue–Langevin, 156 X, F-38042 Grenoble Cédex, France

Abstract. An overall survey of the structural and magnetic features of the $La_2NiO_{4+\delta}$ system is presented as a result of neutron diffraction experiments. The stoichiometric compound ($\delta = 0$) *presents two structural phase transitions. At $T_0 \simeq 770$ K, La_2NiO_4 transforms from tetragonal ($I4/mmm$) to orthorhombic ($Bmab$); at $T_1 \simeq 80$ K, from orthorhombic to a new tetragonal ($P4_2/ncm$) phase.* Associated with this second phase transition a strong microstrain produces anisotropic broadening of Bragg reflections. La_2NiO_4 is three-dimensional (3D) antiferromagnetically ordered at room temperature ($T_N = 330$ K). A weak ferromagnetic component appears below T_1. Oxygen excess suppress the 3D magnetic ordering and the structural phase transformations, giving rise to a non-stoichiometric compound with interstitial oxygens. A tentative phase diagram is proposed.

1. Introduction

In a previous paper dealing with stoichiometric La_2NiO_4 [1] a neutron diffraction experiment as a function of temperature was described. It was shown that a structural phase transition takes place around $T_1 \simeq 80$ K. This transition was characterized by a sudden change in the orthorhombic strain parameter $s = 2(b - a)/(a + b)$ and other structural parameters. The structure was described in the full range of studied temperatures by the same orthorhombic space group $Bmab$. This structure, hereafter called LTO (low-temperature orthorhombic) phase according to [2] and [3], is a distortion of the HTT (high-temperature tetragonal) phase belonging to the space group $I4/mmm$ characteristic of the K_2NiF_4 structural type. The standard setting of $Bmab$ is $Cmca$ but in this work we adopt the common practice in using $Bmab$ as the best description to relate the LTO with the HTT phase. In a recent single-crystal neutron diffraction study on La_2NiO_4, Lander *et al* [4] found that the refinement of the crystal structure at low temperature is better done using the $P4_2/ncm$ space group instead of the orthorhombic $Bmab$. In all of the above references the space group $Pccn$ was not discarded because it gives the same results as $P4_2/ncm$ within the experimental error.

Higher-resolution powder diffraction experiments carried out on nominally stoichiometric samples prepared in different ways were done in order to get a deeper insight into the nature of the low-temperature structural phase transition. The most striking result of these experiments is that the use of conventional Rietveld refinement is unable to fit the whole diffraction profile, whatever space group is used. The reason for this is

the presence of strong anisotropic broadening of reflections due to residual frozen-in microstrain accompanying the phase transition. Meanwhile, Axe *et al* [2, 3] have described a similar phase transition in the related cuprate $La_{2-x}Ba_xCuO_4$, and they proposed that the low-temperature phase is tetragonal (LTT, space group $P4_2/ncm$). This kind of structural phase transition has also been observed in the stoichiometric nickelates Nd_2NiO_4 and Pr_2NiO_4 [5, 6].

There is a renewed interest in K_2NiF_4-type oxides due to the existence of super-conductivity in the cuprates and recently proposed for $La_2NiO_{4+\delta}$ itself [7]. The nature of holes in $La_2NiO_{4+\delta}$ is probably of p character [8] (O^- holes in the p band of oxygens), as in the related cuprates (see [9] and references therein). The origin of hole doping in lanthanum nickelates can depend on the sample preparation method. Two possibilities have been proposed: (i) excess of oxygen as peroxide species or interstitials [8, 10, 11], and (ii) lanthanum vacancies [12]. Our experience is that starting from La : Ni 2 : 1 ratio in air atmosphere, the freshly obtained samples have oxygen excess. However, lanthanum-deficient samples can also be prepared [12] and the reduced samples ($\delta \simeq 0$) are not stable in normal storage conditions. Independently of the particular mechanism actually operating, the usual formulation $La_2NiO_{4+\delta}$ implicitly assumes that oxygen excess is responsible for hole doping in air-prepared La_2NiO_4, and therefore the δ parameter, measured with an appropriate technique, is a useful label to characterize the samples.

The above discussed chemical composition variability is responsible for the changes in physical properties. Transport properties of oxidized samples indicate an evolution from semiconductor to metallic behaviour between 500 and 600 K, and magnetic sus-ceptibility data exhibit rather large variations due to poorly defined compositions (see [1, 13] and references therein). In order to get a deeper insight into the nature of the oxygen defects in the $La_2NiO_{4+\delta}$ structure, several neutron diffraction experiments were carried out on the oxidized compound directly produced by heating the starting oxides at high temperature in air. High-resolution powder diffraction measurements were performed on this oxide and *in situ* reduction in vacuum was followed by neutron thermodiffractometry. The final product was a two-phase material.

From the magnetic point of view, three-dimensional (3D) magnetic order is absent in our oxidized samples, but our two-phase sample clearly shows at 200 K the magnetic reflection (0 1 1). The nearly stoichiometric samples are 3D antiferromagnetically (AF) ordered at room temperature (RT). The magnetic structure agrees with the one reported by Aeppli *et al* [14].

In this paper we give a general survey of the structural features found by high-resolution powder diffraction in different samples of $La_2NiO_{4+\delta}$ oxides. In the case of stoichiometric samples a comparison with our earlier medium-resolution study is made. A detailed description of octahedra tilting and the geometrical relations between the four above-mentioned space groups is given. In addition we discuss the possible magnetic structures (with integral propagation vector, same magnetic and chemical unit cells) which are compatible with *Bmab*, *Pccn* and $P4_2/ncm$ space groups. Finally we shall state the open questions about the suppression of 3D magnetic ordering and the low-temperature phase transition by hole doping.

2. Experimental details

The preparation of $La_2NiO_{4+\delta}$ samples is described elsewhere [15]. The stoichiometric compound is obtained by reduction of the oxidized precursor (obtained by standard

ceramic procedures) at a relatively low temperature (510 K) under a dry hydrogen atmosphere, and careful monitoring of the reduction process by thermogravimetry. In the stoichiometric compound no Ni^{3+} can be detected by titration techniques.

We will concentrate on three different kind of samples:

(i) The fully oxidized precursor as obtained in air at 1523 K (O).

(ii) A partially oxidized sample (P), obtained from O in the course of a neutron diffraction experiment carried out at high temperature under vacuum.

(iii) Stoichiometric samples (S), prepared by reducing up to nominal stoichiometry.

In the latter case, two reduced samples (S1 and S2) were prepared by standard ceramic procedures and reduced in a H_2 flow. The only difference was the annealing time at high temperature in air atmosphere. This time was about twice as long for the S1 sample.

The neutron diffraction experiments were carried out in Grenoble at the Institut Laue-Langevin on the D1B ($\lambda \simeq 2.52$ Å), D1A ($\lambda \simeq 1.91$ Å) and D2B ($\lambda \simeq 1.59$ Å) powder diffractometers and on the IN20 triple-axis spectrometer in order to perform a separation of the magnetic scattering by using polarization analysis. Standard 'orange' cryostats were used for studies at low temperature and furnaces with vanadium resistors for the high-temperature experiments.

The data were analysed by using the programs existing in the STRAP package [16], and in particular the program FULLPROF [17]. This program allows the Rietveld refinement of multiphase patterns combining nuclear and magnetic structures. The treatment of the anisotropic broadening found at low temperature in the S samples has been done by introducing a subroutine in which the particular *hkl* dependence of the contribution to the FWHM of reflections is described with only one adjustable parameter. A detailed description of the formalism used to describe anisotropic microstrain is presented in the appendix.

3. Results and discussion

3.1. Crystallographic descriptions of the Ln₂NiO₄ compounds

The lanthanide nickelates belong to the family of compounds with a structure related to the K_2NiF_4 type. Several studies can be found in the recent literature dealing with the structural phase transitions and polymorphism in such structures [18, 19]. In our case we are only interested in the structures derived from the parent $I4/mmm$ space group by condensation of the soft mode with wavevector corresponding to the X point of the Brillouin zone (BZ). The order parameter is two-dimensional (2D) owing to the degeneracy of the X point. Depending on the particular relations between the two components of the order parameter, we obtain one of the following space groups: *Bmab*, *Pccn* and *P4₂/ncm*. For simplicity, and in order to get a better comparison between the structural parameter of the different phases, we use the F-centred cell for the parent structure. Therefore, the non-conventional symbol $F4/mmm$ for the standard $I4/mmm$ space group will be used.
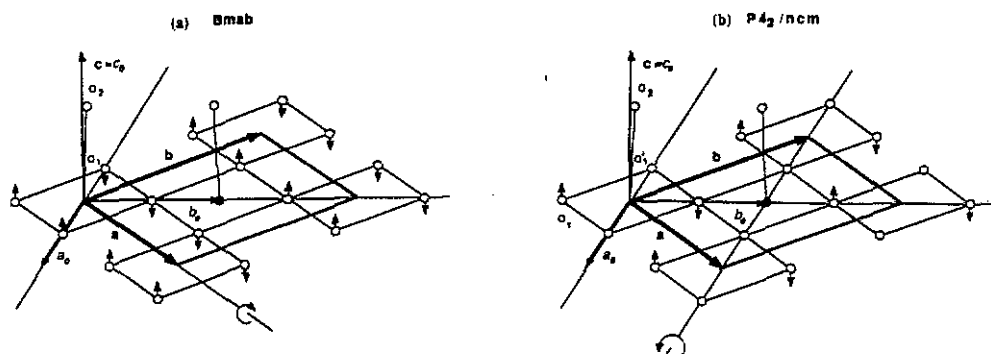
The Wyckoff positions occupied by atoms in compounds of formula Ln_2MO_4 with the above-mentioned space groups are given in table 1. In figure 1 we show the oxygen displacements from the HTT needed to give the different derived structures that can be described by orthorhombic *Pccn* and *Bmab* or by tetragonal *P4₂/ncm* space groups. The

Table 1. Positions occupied [a] by atoms in Ln_2NiO_4 in space groups $F4/mmm$[b], $Bmab$, $P4_2/ncm$ and $Pccn$.

	$F4/mmm$		$Bmab$		$P4_2/ncm$		$Pccn$	
La	(8e) $4mm$	(00z)	(8f) $m..$	(0yz)	(8i) $..m$	(xxz)	(8e) 1	(xyz)
Ni	(4a) $4/mmm$	(000)	(4a) $2/m..$	(000)	(4d) $..2/m$	(000)	(4a) $\bar{1}$	(000)
O1	(8c) mmm	($\frac{1}{4}\frac{1}{4}$0)	(8e) $..2$	($\frac{1}{4}\frac{1}{4}$z)	(4e) $2.mm$	($\frac{1}{4}\frac{1}{4}$z)	(4c) $..2$	($\frac{1}{4}\frac{1}{4}$z)
O1'					(4a) 2.22	($\frac{1}{4}\frac{3}{4}$0)	(4a) $..2$	($\frac{1}{4}\frac{3}{4}$z)
O2	(8e) $4mm$	(00z)	(8f) $m..$	(0yz)	(8i) $..m$	(xxz)	(8e) 1	(xyz)

[a] In parentheses we give the multiplicity and Wyckoff letter of the site, followed by the local point symmetry and the first equivalent position coordinates. The approximate values of coordinates for each atom can be given in $Pccn$, which is a subgroup of the others: for La, $x \approx y = 0, z = 0.364$; for basal oxygens O1 and O1', $z \approx 0$; and for apex oxygen O2, $x \approx y \approx 0, z \approx 0.175$.

[b] The tetragonal high-temperature phase is described in the face-centred tetragonal space group, which is exactly the same as $I4/mmm$ but with the unit-cell setting compatible with the remaining low-symmetry phases: $a_F = a_1 + b_1, b_F = a_1 - b_1, c_F = c_1$. In this case we have kept the same Wyckoff letters as in $I4/mmm$, changing only the multiplicity.

Figure 1. Oxygen displacements in the NiO_2 plane for the two space groups: (a) orthorhombic, $Bmab$; (b) tetragonal, $P4_2/ncm$.

less symmetric space group is $Pccn$, which is a subgroup of all the others. $Bmab$ and $P4_2/ncm$ are both subgroups of the parent $F4/mmm$, but $P4_2/ncm$ is not a subgroup of $Bmab$.

3.2. The crystal structure of air-oxidized $La_2NiO_{4+\delta}$: interstitial oxygens

In earlier literature, the air-synthesized $La_2NiO_{4+\delta}$ was the prototype of the K_2NiF_4-structural type in the oxides. It is clear that the use of x-ray diffraction (XRD) is not sufficient as a characterization tool for the structure of this oxide. In fact XRD shows just the average tetragonal structure without any particular problem. However, when one tries to refine the crystal structure by the Rietveld method from a neutron powder diffraction pattern using the standard K_2NiF_4 type, it is evident that something is wrong in this assumption.

The introduction of oxygen excess in the positions suggested by Ganguly *et al* [11] has a significant effect in the improvement of the goodness of fit. The R_{Bragg} goes down from 7.3% to 4.1% (R_{wp} from 16.4% to 13.9%). We have applied the same constraints

on the site occupancies and oxygen displacements as Chaillout *et al* [20] for $La_2CuO_{4+\delta}$ and Jorgensen *et al* [10] for $La_2NiO_{4+\delta}$. The reasons for the application of such constraints are very well explained in the above-mentioned papers and so they will not be discussed here. To make some comparisons we have also studied the oxygen excess model proposed by Kajitani *et al* [21] in the space group $P4_2/ncm$. In our case, the refinement in $P4_2/ncm$ gives nearly the same results as in $F4/mmm$. Moreover, all the free extra structural parameters (x position of La, for instance) fit, within the standard deviations, to the corresponding values in the $F4/mmm$ space group. We have also compared the orthorhombic (*Fmmm*) model proposed by Jorgensen *et al* [10] with the tetragonal $F4/mmm$. The use of the orthorhombic space group is better than the unstrained tetragonal space group. However, applying a model for the microstrains induced by the interstitial oxygens (see appendix) we were able to fit properly the diffraction pattern in the tetragonal space group.

In table 2 we give the final structural parameters at 1.5 K for the O sample, as well as some important distances. The composition obtained from the refinement was $La_2NiO_{4.15(1)}$. The shortest distance between the interstitial oxygen and the displaced one at 1.5 K is 1.65 Å, which is very similar to the corresponding one for La_2CuO_4 [20], 1.64 Å. This distance may suggest the existence of a peroxide species $(O_2)^{2-}$, as found in BaO_2 (O–O distance of 1.5 Å). The corresponding value of the distance from Jorgensen *et al* [10] ($\delta \simeq 0.18$) is 1.62 Å (not given in their paper), in good agreement with our value.

3.3. The crystal structure of partially oxidized $La_2NiO_{4+\delta}$: a two-phase sample

The structure refinement of the P sample can only be done by assuming a two-phase model. In this point we confirm the results obtained by Jorgensen *et al* [10] concerning the disproportionation in two phases for intermediate overall oxygen excess. The fit of the diffraction pattern at 180 K has been carried out using the two phases ($F4/mmm$ and *Bmab*). The results of the refinement are shown in table 2, the total oxygen stoichiometry is $\delta \simeq 0.07$. The quality of the refinement is poorer than in the other cases presented in this paper, and this is due to inhomogeneities of the oxygen excess distribution inside the sample; therefore the fitted structural parameters have to be considered with caution. We consider that the use of the two-phase mixture ($F4/mmm$ and *Bmab*) to fit the diffraction pattern is only a crude approximation to the actual structure/microstructure of such samples. A more realistic situation could be the following: in regions of high oxygen content the octahedra tilt is prevented, and the corresponding structures are of $F4/mmm$ or *Fmmm* type. When the oxygen excess is scarce, the octahedra are tilted and regions with structures of the *Bmab* type develop.

Another point that confirms the former idea is the fact that the *Bmab* phase for this mixture sample has a bigger volume (0.4%) than the corresponding stoichiometric pure phase, at the same temperature. In principle, some interstitial oxygens could exist in this *Bmab* phase, which have not been taken into account.

3.4. The crystal structure of stoichiometric La_2NiO_4 between 100 K and room temperature

The crystal structure of stoichiometric La_2NiO_4 between 100 K and room temperature (RT) is orthorhombic *Bmab*. The results of the neutron diffraction patterns refinements at 250 and 120 K (D1A, $\lambda \simeq 1.9$ Å) are summarized in table 3. In figure 2(a) we show a plot of the observed and calculated diffraction patterns for $T \simeq 120$ K.

Table 2. Refined parameters for La₂NiO₄₊δ at 1.5 and 180 K.

	1.5 K					180 K									
Temperature	F4/mmm					F4/mmm					Bmab				
Space group	0.15(1)					0.10(2)					<0.02 (overall 0.07)				
Excess of oxygen (δ)	99.8					66.9					32.8				
Abundance (%)															
Atom[a]	Site	x	y	z	B (Å²)	Site	x	y	z	B (Å²)	Site	x	y	z	B (Å²)
La	8e	0	0	0.3611(1)	0.29(2)	8e	0	0	0.3622(3)	0.57(4)	8f	0	−0.012(1)	0.3657(7)	0.57(4)
Ni	4a	0	0	0	0.30(2)	4a	0	0	0	0.55(4)	4a	0	0	0	0.55(4)
O1	8c	¼	¼	0	0.70(4)[c]	8c	¼	¼	0	0.55(5)	8c	¼	¼	−0.0160(9)	0.55(5)
O2	8e	0	0	0.1735(3)	0.61(5)	8e	0	0	0.1772(9)	0.6(1)	8f	0	0.053(2)	0.179(1)	0.80(6)
O_I	8e	¼	¼	0.2416(5)	0.61(5)	8e	¼	¼	0.2500(0)	0.6(1)	—				—
O_D	—	−0.066(1)	−0.066(1)	0.1751(1)	0.61(5)	—	−0.062(5)	−0.062(5)	0.175(5)	0.6(1)	—				—
a (Å)	5.45514(4)					5.4897(3)					5.4618(5)				
b (Å)						5.4897(3)					5.4967(5)				
c (Å)	12.6461(1)					12.5708(7)					12.561(2)				
ε = 0.00039(2)															
R_Bragg (%)	4.09					4.28					7.42				
R_wp (%)	9.26					11.6									
R_exp (%)	3.28					4.28									
Distances (Å)															
Ni–O1 [×4]	1.9287(0)					1.9409(1)					1.948(1)				
Ni–O2 [×2]	2.194(4)					2.23(1)					2.27(2)				
O_I–O_D	1.77(3)					1.74(4)					—				
O_I–O_D	1.65(3)					2.21(4)					—				

[a] A small quantity of NiO was included in the refinements.

[b] Subscripts I and D stand for 'interstitial' and 'displaced'. The occupation numbers of the O2, O_I and O_D are calculated applying the following restriction for the total number (n) of oxygens per unit formula: $n(O2) = 2 − n(O_D)$. $n(O_D) = 4n(O_I) = \delta$. The fitted value of $n(O_I) = \delta$ is 0.151(9) for O sample.

[c] This parameter was refined anisotropically; the rms displacements are 0.073 Å in the ab plane, and 0.127 Å along the c axis.
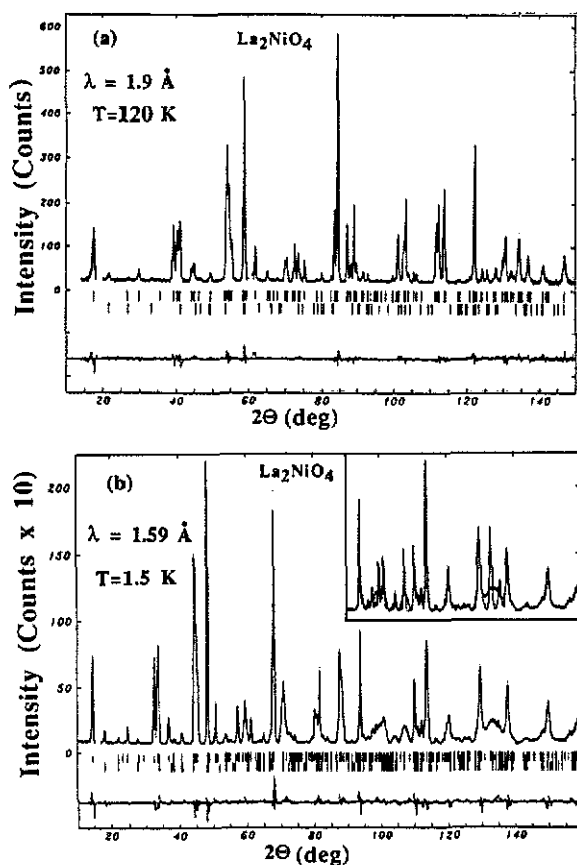
Table 3. Refined parameters for stoichiometric La$_2$NiO$_4$ at 1.5, 120 and 250 K.

Temperature Space group		1.5 K P4$_2$/ncm				120 K Bmab				250 K Bmab			
Atom	Site	x	y	z	B (Å²)	Site	x	y	z	B (Å²)	Site	x	y	z	B (Å²)
La	8i	−0.0072(3)	−0.0072(3)	0.3639(1)	0.26(3)	8f	0	−0.0102(3)	0.3639(1)	0.16(5)	8f	0	−0.0099(5)	0.3634(1)	0.36(7)
Ni	4d	0	0	0	0.30(3)	4a	0	0	0	0.23(5)	4a	0	0	0	0.31(6)
O1	4e	¼	¼	−0.0155(4)	0.07(8)	8e	¼	¼	−0.0109(2)	0.37(5)	8e	¼	¼	−0.0095(3)	0.40(7)
O1'	4a	¼	¾	0	0.43(9)	−	−	−	−	−	−	−	−	−	−
O2	8i	0.0314(3)	0.0314(3)	0.1771(2)	0.44(4)	8f	0	0.0417(3)	0.1771(2)	0.63(5)	8f	0	0.0397(6)	0.1778(2)	0.98(8)
	a (Å)	5.4995(1)				a (Å)	5.4419(1)				a (Å)	5.4499(2)		
						b (Å)	5.5364(1)				b (Å)	5.5275(2)		
	c (Å)	12.5052(2)				c (Å)	12.4896(2)				c (Å)	12.5118(3)		
	ε = 0.00586(4)													
Magnetic moment (μ_B)		1.68(6)					1.58(6)					1.36(7)		
R_{Bragg} (%)		4.52 (11.9 magnetic)					3.92 (17.1 magnetic)					4.26 (25.8 magnetic)		
R_{wp} (%)		8.75					7.76					8.28		
R_{exp} (%)		3.18					5.69					6.80		

Distances (Å) and angles (deg)

	1.5 K		120 K		250 K
Ni–O1 [×2]	1.9540(5)	Ni–O1 [×4]	1.9456(2)	Ni–O1 [×4]	1.9442(2)
Ni–O1' [×2]	1.9444(0)				
Ni–O2 [×2]	2.2281(3)		2.224(2)		2.235(2)
Ni–O1–Ni	168.6(2)		172.0(1)		173.0(2)
Ni–O1'–Ni	180.0				

Figure 2. Diffraction patterns of La_2NiO_4 at different temperatures: (*a*) 120 K and (*b*) 1.5 K. Inset in (*b*) shows the refined diffraction pattern without microstrain parameter (see appendix). The lowest row of vertical marks corresponds to the allowed magnetic reflections.

From the point of view of the geometrical features of the Ni octahedra, the main aspect to be stressed is that the difference between α_1 and α_2 angles is lower than that obtained in [1]. Therefore, one can assume that the octahedra tilt is nearly rigid. The stronger difference found in [1] was mostly due to the fact that the individual temperature factors were not refined due to an insufficient Q resolution from the data of the D1B diffractometer. If one uses the angle $\omega = \frac{1}{2}(\alpha_1 + \alpha_2)$ as a measure of the order parameter (rigid tilt around $[100]_{LTO}$) corresponding to the structural phase transition $I4/mmm \rightarrow Bmab$ (see section 3.5), on going from 250 to 120 K the angle changes from 5.3 to 5.8°. In the same way, a slight increase (0.7%) in the distance Ni–O1 as well as a decrease of the distance Ni–O2 (0.5%) is observed. The angle $\omega_{[100]}$ might have a critical value for the *Bmab* structure to be stable. Then, tilt angles greater than the critical value destabilize the system and a phase transition occurs in order to rearrange the structure. From the temperature dependence of the lattice parameters below room temperature, thermal expansion coefficients of the LTO phase have been calculated using the expression: $\alpha = L^{-1}(T) \, dL/dT = A + BT$ [22]. The values of the A and B coefficients are: $1.13 \times 10^{-5}\,\text{K}^{-1}$, $-1.28 \times 10^{-10}\,\text{K}^{-2}$ along the *a* axis, $-6.44 \times 10^{-6}\,\text{K}^{-1}$,
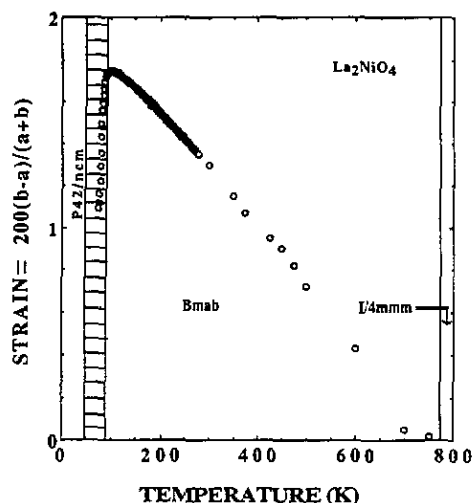
Figure 3. Dependence of the orthorhombic strain with temperature, showing two structural phase transitions at $T_1 \simeq 80$ K and $T_0 \simeq 770$ K. The vertical lines indicate the structural phase transitions. The shaded area around 80 K indicates the region of coexistence of both phases (LTO and LTT).

$-4.15 \times 10^{-11}\,\mathrm{K}^{-2}$ along the b axis, and $1.48 \times 10^{-5}\,\mathrm{K}^{-1}$, $-2.17 \times 10^{-10}\,\mathrm{K}^{-2}$ along the c axis.

3.5. The structural phase transitions in stoichiometric La₂NiO₄

The experimental results concerning the structural behaviour of La₂NiO₄ as a function of temperature are shown in figure 3, where the orthorhombic strain is plotted versus temperature. Two structural phase transitions are clearly visible in this temperature range. First, at $T_0 \simeq 770$ K, there is a transformation from $F/4mmm$ to $Bmab$, which is a transition of second-order type. At low temperature, the system transforms to a new structure at $T_1 \simeq 80$ K. The transformation to the low-temperature phase is strongly first-order. We have reanalysed the data of D1B [1] introducing two phases (see below), $P4_2/ncm$ and $Bmab$, fixing their atomic positions to the values found in the high-resolution experiments, and fitting only the cell parameters and scale factor of both phases. Performing a cyclic Rietveld refinement, we have obtained the relative fraction of each phase as a function of the temperature (figure 4). The results show the existence of a wide temperature range (50 to 95 K) where both phases (LTO and LTT) coexist. The obtained behaviour indicates that the tetragonal phase begins to nucleate at around 95 K and grows progressively on cooling down at the expense of the orthorhombic phase. Because of the first-order character, there is a phase coexistence in a wide temperature range. For that reason, the orthorhombic strain associated with the $Bmab$ phase exists even at temperatures lower than T_1. We have considered as the transition temperature the point at which 50% of the new phase $(P4_2/ncm)$ occurs, i.e. $T_1 \simeq 80$ K (figure 4).

As a model for the phase transitions that can exist in La₂NiO₄ due to nearly rigid octahedra tilts, one can give the two most probable sequences of transitions:

(i) $I4/mmm \rightarrow Bmab \rightarrow P4_2/ncm$,
(ii) $I4/mmm \rightarrow Bmab \rightarrow Pccn$.

These sequences of transitions in K₂NiF₄-type compounds were predicted from theoretical group analysis by Petzelt [18] and Alexandrov [19] and were explained in the
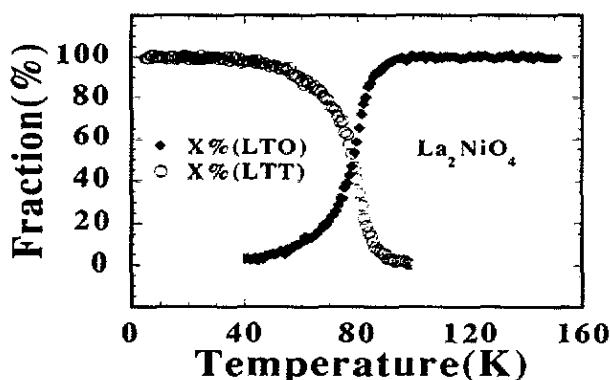
Figure 4. Temperature dependence of the molar fraction of the LTO (*Bmab*) and LTT ($P4_2/ncm$) phases for stoichiometric La_2NiO_4.

framework of Landau's phenomenological theory of phase transitions and applied to compounds of formula $(C_nH_{2n+1}NH_3)_2MCl_4$ (M = Cu, Mn, Fe, Cd). Recently, Axe *et al* [2, 3] have applied the same type of analysis to $La_{2-x}Ba_xCuO_4$.

From the different sequences of transitions presented above, the more likely to be fulfilled experimentally is the first one. In the following we will try to justify this statement. Starting from HTT, the *Bmab* phase appears as the consequence of the doubly degenerate soft-mode condensation at the X point $[\frac{1}{2}\frac{1}{2}0]$ on the Brillouin zone of the HTT phase. If we call Q_1 and Q_2 the amplitudes (two-dimensional order parameters) of the normal modes corresponding to the wavevectors $q_1 = [\frac{1}{2}\frac{1}{2}0]$ and $q_2 = [\frac{1}{2}-\frac{1}{2}0]$ of the $I4/mmm$ structure, the LTO phase corresponds to $Q_1 \neq 0$ and $Q_2 = 0$, or $Q_1 = 0$ and $Q_2 \neq 0$. The two possibilities describe two types of domains, which have to be present in twinned crystallites. The hypothetical phase transition HTT → LTT corresponds to $Q_1 = Q_2 \neq 0$. Another hypothetical possibility is the transition HTT → LTO' (*Pccn*), which corresponds to $Q_1 \neq Q_2 \neq 0$. The pattern of basal oxygen atom displacements corresponding to LTO (rotation along $[100]_{LTO} = [110]_{HTT}$) and LTT (rotation along $[110]_{LTT} = [100]_{HTT}$) is shown in figures 1(*a*) and (*b*), respectively. The displacements for LTO' (rotation along an intermediate axis) are similar to LTO, but with different values of the shift for opposite basal oxygens along one octahedron edge. All these transitions could be of second-order character as a group–subgroup relationship exists.

In the two sequences mentioned above ((i) and (ii)) the first transition $I4/mmm →$ *Bmab* takes place for La_2NiO_4 at $T_0 \simeq 770$ K; the transition seems to be continuous (second-order). The phase transition at $T_1 \simeq 80$ K could correspond to the second transition of sequence (ii). However, for this case the existence of a group–subgroup relationship (*Bmab* ⊃ *Pccn*) could imply a second-order transition. As the change in the unit cell is quite sudden, the sequence (i) is more likely. This transition corresponds ideally to the case $Q_1 = Q_2 \neq 0$ (referred to the normal modes of the HTT). However, coming from the *Bmab* phase where twins exist, and therefore structural defects are present, the exact relation $Q_1 = Q_2$ is only fulfilled on average (macroscopic distances). Locally, a gap $\Delta = Q_1 - Q_2 \neq 0$ exists, which has $\langle \Delta \rangle = 0$ but $\langle \Delta^2 \rangle \neq 0$, where $\langle \ \rangle$ indicates spatial average. The value of $\langle \Delta^2 \rangle$ may depend on the preparation method or on the thermal history of the sample.

From a structural point of view Q_i is related to the z coordinates of the oxygens belonging to the NiO_2 planes. Moreover, the following relationships can be established (see also table 1):

$$Bmab \rightarrow Q_1 = 0, Q_2 \neq 0 \rightarrow z(O1') = z(O1) \neq 0 \rightarrow a \neq b, |a - b|_{LTO}(\text{max})$$
$$\rightarrow \text{tilt axis } [1\,0\,0]$$
$$P4_2/ncm \rightarrow Q_1 = Q_2 \neq 0 \rightarrow z(O1') = 0, z(O1) \neq 0 \rightarrow a = b, |a - b|_{LTT} = 0$$
$$\rightarrow \text{tilt axis } [1\,1\,0]$$
$$Pccn \rightarrow Q_1 \neq Q_2 \neq 0 \rightarrow z(O1') \neq z(O1) \neq 0 \rightarrow a \neq b, |a - b|_{LTO'} < |a - b|_{LTO}$$
$$\rightarrow \text{tilt axis } [u\,v\,0].$$

In a diffraction experiment the analysis of the integrated intensities of Bragg peaks reveals only a spatial average. This fact explains why Lander *et al* [4] found that nothing is gained in refining the structure in the *Pccn* space group instead of $P4_2/ncm$ in a single-crystal experiment. However, a diffraction experiment is able to show that $\langle \Delta^2 \rangle \neq 0$ by an indirect way: the presence of anisotropic broadening of the Bragg reflections due to correlated fluctuations of the cell parameters.

The presence of twins implies that the a and b axes of the *Bmab* phase alternate from one domain to another, along two perpendicular directions X and Y associated with a crystallite. Some of the planes $\{1\,1\,0\}_{LTO}$ constitute the domain walls. This means that the tilt axis ($[1\,0\,0]_{LTO}$) of the NiO₆ octahedra changes by 90° on going from one domain to another. When the LTO to LTT phase transition takes place, the twin boundaries act as breaking elements in the long-range coherence of the new tilt axes ($[1\,1\,0]_{LTT}$) in the plane $z = 0$ and $[1\,\bar{1}\,0]_{LTT}$ in the plane $z = \frac{1}{2}$), introducing a sort of 'signature' of the old microstructure in the new growing phase. For instance, in the middle of two adjacent domains, where perfect tetragonal symmetry exists, the tilt axes at the same NiO₂ plane could be orthogonal. The connection between the two regions is performed by a continuous change in the orientation of the local tilt axes, which produces the local microstrain. This model of the origin of microstrain suggests that samples with low density of twin boundaries must have smaller microstrain.

Experimentally, no discontinuity in the cell volume, as well as in the c axis, is observed at the phase transition. The observed discontinuity takes place only in the ab plane, but, in order to fulfil the relation $V_{LTO} = V_{LTT}$ at $T = T_1$, the area S_{ab} must be conserved up to first order in the strains. As a consequence, the local orthorhombic cells $(a_l, b_l$ and $c_l)$ must everywhere satisfy the relations $a_l = a_T(1 - \varepsilon_l)$, $b_l = a_T(1 + \varepsilon_l)$ and $c_l = c_T$, where the subscript T stands for the average tetragonal cell and ε_l for the local microstrain. This model implies that the fluctuations of the average cell parameter a_T are the same along the X and Y directions (global tetragonal symmetry) and the local correlation is negative and the highest (100%). A particular sample can be characterized by giving the root-mean-square microstrain parameter as a measurement of the cell parameter fluctuations $\varepsilon = \sigma/a_T = \langle \varepsilon_l^2 \rangle^{1/2}$. The effect produced by these fluctuations and correlation on the width of the Bragg reflections is derived in the appendix.

3.6. The crystal structure of stoichiometric La₂NiO₄ at 1.5 K

Using the Rietveld method adapted for handling anisotropic broadening we have refined the structure of La₂NiO₄ at low temperature for the two stoichiometric samples prepared in different ways. The results of the refinement for the S2 sample are shown in table 3. Figure 2(b) presents a plot of the observed and calculated diffraction patterns. The refinement of the S1 sample gave the same structural parameters within standard deviations. The only difference was the value of the microstrain parameter, which was lower

for the S1 sample ($\varepsilon = 0.00437(3)$ compared with $\varepsilon = 0.00586(4)$ for S2). Comparing the inset of figure 2(*b*) with the global pattern, one can see the dramatic effect of the introduction of the model for anisotropic broadening of the Bragg reflections described in the appendix. The tilt axis of the Ni octahedra is now around [1 1 0] in the $z = 0$ plane and around [1 $\bar{1}$ 0] in the $z = \frac{1}{2}$ plane; the value of $\omega_{[110]}$ is $\simeq 6°$.

One important difference between LTO and LTT phases is that, in the second one, the basal oxygens of the nickel octahedron are no longer equivalent and two different distances exist (Ni–O1 and Ni–O1'). The Ni–O1' distance is very close to the value of Ni–O1 in the *Bmab* phase at 120 K. However, the Ni–O1 distance is 0.43% bigger than the corresponding one in the LTO phase. As a consequence, the stretching vibrational modes have two different frequencies. This effect was actually observed in the IR spectrum of the Ln_2NiO_4 compounds (Ln = La, Pr and Nd) [23]. At high temperature (LTO phase) only one IR band is observed in relation with the in-plane stretching vibrations of the Ni–O atoms of the equatorial plane of the octahedra (663 cm^{-1}); while at low temperature (LTT phase), the above-mentioned IR band is split (667 and 655 cm^{-1}).

In the case of the Ni–O2 distance (apical oxygen) there is a slight increase of 0.18% between the LTO phase at 120 K and the LTT phase at 1.5 K. The thermal expansion coefficients of the LTT phase calculated between 1.5 and 50 K [23] give $B \simeq 0$ and A values of 1.7×10^{-6} K^{-1} and $\simeq 0$ along a and c axes, respectively.

3.7. Magnetic structure of the stoichiometric sample

The magnetic origin of the (0 1 1) reflection in S samples was clear from the beginning of the experiments owing to its evolution as a function of temperature. To be sure of its magnetic origin, an experiment with polarized neutrons and full polarization analysis was done on IN20. The neutrons were polarized in such a manner that the polarization vector was always parallel to the scattering vector; the *spin-flip* and *spin-non-flip* cross sections were measured. With this geometrical set-up the pure nuclear scattering is *non-spin-flip* and the pure magnetic scattering is *spin-flip*. In figure 5 we show the results of this experiment carried out at room temperature (the small spin-flip observed for the (0 0 2) reflection is due to a non-perfect flipping ratio). The magnetic origin of the (0 1 1) reflection is clearly established.

Neutron powder diffraction experiments support unambiguously a magnetic structure that is well described by the antiferromagnetic mode g_x (propagation vector $k =$ [1 0 0], representation $\Gamma_{7g}(- - +)$, see below). If we number the magnetic atoms as Ni_1 $(0, 0, 0)$, Ni_2 $(\frac{1}{2}, 0, \frac{1}{2})$, Ni_3 $(0, \frac{1}{2}, \frac{1}{2})$ and Ni_4 $(\frac{1}{2}, \frac{1}{2}, 0)$, the mode corresponds to the spin arrangement $g_x = s_{1x} - s_{2x} + s_{3x} - s_{4x}$, and the Ni spins are in the direction [1 0 0], which is the direction of the tilt axis of NiO_6 octahedra. The conditions limiting possible magnetic reflections for this model are easily obtained from the expression for the magnetic unit-cell structure factor: $h = 0$, k and l odd. For all the other cases the magnetic intensity is zero, and for the allowed reflections the following expression holds: $I_M(Q) \simeq 16[\mu f(Q)]^2$, where Q is the modulus of the scattering vector, μ is the magnetic moment and $f(Q)$ is the normalized magnetic form factor for the free ion Ni^{2+}. The magnetic form factor we have used in the calculations has been taken from [24]. The first and the most intense calculated magnetic reflection is (0 1 1), as is actually observed. This magnetic structure corresponds with the one proposed by Aeppli *et al* [14] for a slightly oxidized sample and the magnetic structure found by Lander *et al* [4] in a stoichiometric single crystal. A schematic representation of the magnetic structure is included as an inset in figure 6.
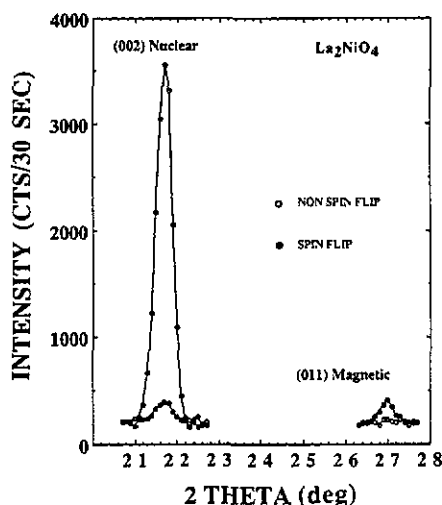
Figure 5. Polarized beam diffraction pattern, for a restricted angular range, which includes a strong nuclear reflection (002) and a magnetic reflection (011) showing that it is indeed magnetic in origin.
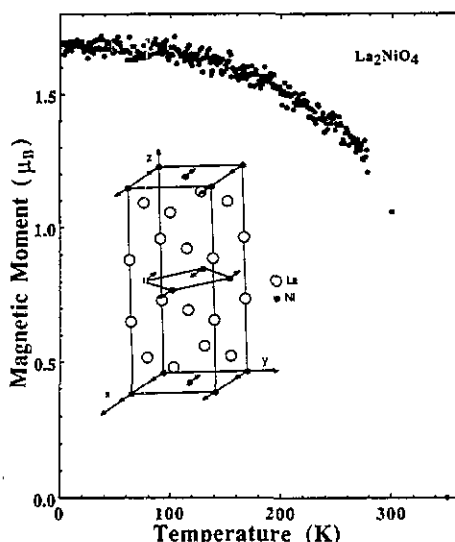

Figure 6. Temperature dependence of the magnetic moment for La₂NiO₄, from data of the (011) magnetic reflection. Inset shows the proposed magnetic structure.

This magnetic model was introduced in the structure refinement in order to get the value of the magnetic moment at different temperatures. In figure 6 we represent the evolution of the magnetic moment as a function of temperature as obtained from the analysis of D1B data on the magnetic reflection (011). The extrapolation of the data gives a transition temperature of about $T_N = 330$ K. The expected 2D magnetic scattering cannot be detected because in the powder samples the magnetic reflections are too weak near the Néel point. It may be noticed that no anomaly is seen when the sample undergoes the structural phase transition around 80 K. The value of the magnetic moment, $1.68 \pm 0.06 \, \mu_B$ at 4 K, is lower than the saturation (spin-only) moment of high-spin $Ni^{2+}(d^8)$. This spin reduction is mainly due to zero-point quantum fluctuations, which are enhanced in 2D Heisenberg antiferromagnetic systems. This value is in good agreement with the value ($1.68 \, \mu_B$) obtained by Lander *et al* [4].

The same kind of experiments were carried out on O and P samples. In O samples we have not detected any evidence of long-range magnetic ordering. In the P sample the (011) reflection becomes noticeable at 200 K ($T_N \approx 230$ K), but, as we have seen above, it was a two-phase sample.

The magnetic structure is different from the corresponding one for La₂CuO₄, which has a magnetic structure belonging to representation $\Gamma_{4g}(-++)$ of the *Bmab* space group. In table 4 we give the one-dimensional representations, with their corresponding basis functions, to which the magnetic structures compatible with the space groups *Bmab*, *Pccn* and *P4₂/ncm* belong. To derive these representations we have applied the macroscopic theory established by Bertaut [25]. As independent symmetry elements we have used the generators given in table 4, and the magnetic modes.

$$f = s_1 + s_2 + s_3 + s_4 \qquad g = s_1 - s_2 + s_3 - s_4$$

$$c = s_1 + s_2 - s_3 - s_4 \qquad a = s_1 - s_2 - s_3 + s_4.$$

Table 4. Basis functions (magnetic modes) of irreducible representations for Ni sites in *Bmab*, *Pccn* and *P4₂/ncm* space groups. The '*j*' representation is labelled by the symbol Γ_j. The + and − symbols in parentheses correspond to the characters +1 or −1 of the space group generators. As Ni sites are in inversion centres only the *gerade* (even) representations are considered. The Shubnikov group symbol (SS) is also given.

(*a*) *Bmab*

$\{B, 2_{1y}, 2_z\}$	SS	x	y	z
$\Gamma_{1g}(+\,+\,+)$	*Bmab*	c_x	–	–
$\Gamma_{2g}(+\,+\,-)$	*Bm'ab*	–	f_y	c_z
$\Gamma_{3g}(+\,-\,+)$	*Bm'a'b*	–	c_y	f_z
$\Gamma_{4g}(-\,+\,+)$	$B_p m'a'b'$	–	g_y	a_z
$\Gamma_{5g}(+\,-\,-)$	*Bma'b'*	f_x	–	–
$\Gamma_{6g}(-\,+\,-)$	$B_p ma'b$	a_x	–	–
$\Gamma_{7g}(-\,-\,+)$	$B_p mab'$	g_x	–	–
$\Gamma_{8g}(-\,-\,-)$	$B_p m'ab$	–	a_y	g_z

(*b*) *P4₂/ncm*[*]

$\{2_{1y}, 2_z, 4_{2z}\}$	SS	x, y	z
$\Gamma_{1g}(+\,+\,+)$	*P4₂/ncm*	$c_x - g_y$	–
$\Gamma_{2g}(+\,+\,-)$	*P4'₂/ncm'*	$c_x + g_y$	a_z
$\Gamma_{3g}(-\,+\,+)$	*P4₂/nc'm'*	$g_x + c_y$	f_z
$\Gamma_{4g}(-\,+\,-)$	*P4'₂/nc'm*	$g_x - c_y$	–

[*] The remaining two-dimensional representation is not given.

(*c*) *Pccn*

$\{2_{1y}, 2_z\}$	SS	x	y	z
$\Gamma_{1g}(+\,+)$	*Pccn*	c_x	g_y	a_z
$\Gamma_{2g}(+\,-)$	*Pc'cn'*	a_x	f_y	c_z
$\Gamma_{3g}(-\,+)$	*Pc'c'n*	g_x	c_y	f_z
$\Gamma_{4g}(-\,-)$	*Pcc'n'*	f_x	a_y	g_z

The numbering of Ni atoms is given above. It is clear from table 4 that weak ferromagnetism cannot exist in connection with a g_x mode above the low-temperature structural phase transition. This is important in order to explain the magnetic properties of stoichiometric La_2NiO_4. The situation is different below T_1. Even if at low temperature the average crystal structure is tetragonal, the magnetic symmetry can be orthorhombic. In such a case the relevant space group to perform the representation analysis of the low-temperature phase is *Pccn*, and the representations $\Gamma_{7g}(-\,-\,+):g_x$ and $\Gamma_{3g}(+\,-\,+):c_y f_z$ of *Bmab* are mixed to give the representation $\Gamma_{3g}(-\,+):g_x c_y f_z$ of *Pccn*, which allows the existence of a ferromagnetic component along the c axis. Our experiment is not sensitive enough to detect the weak components c_y and f_z.

If the magnetic symmetry were tetragonal at low temperature, the main spin directions should not be colinear and the magnetic structure corresponds to the representation $\Gamma_{3g}(-\,+\,+):g_x + c_y f_z$. Powder diffraction cannot distinguish between the tetragonal and
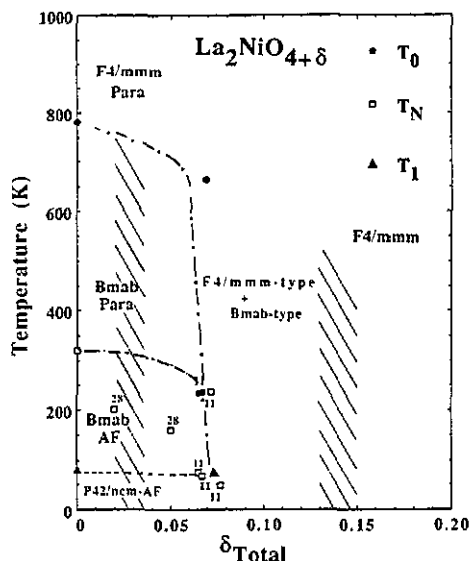
Figure 7. Structural and magnetic phase diagram for La₂NiO₄₊δ depending on the doping concentration of oxygen (low-concentration side). δ is the total oxygen content. Vertical marks indicate the tentative phase boundary for oxygen solubility. Numbers in the figure indicate the corresponding references.

orthorhombic magnetic ordering, as both spin arrangements give exactly the same intensities.

3.8. Tentative phase diagram for La₂NiO₄₊δ

A tentative phase diagram is presented in figure 7. The task to reproduce the oxygen content phase diagram in La₂NiO₄₊δ is very difficult because of the lack of reliable and systematic data. Although the qualitative features are clear, the correct place for the phase boundaries is not yet well determined. The best known is the low-concentration side of the phase diagram. The stoichiometric compound is single-phase and presents three phase transitions in the range 1.5 to 1000 K: two structural changes, at 770 K from $I4/mmm$ to $Bmab$ and from $Bmab$ to $P4_2/ncm$ at 80 K; and the 3D antiferromagnetic ordering of the Ni sublattice at around 330 K. These phase transformations can be followed until $\delta = 0.09$, where both high-temperature structural and magnetic phase transitions disappear.

In the intermediate oxygen concentration range $0.02 < \delta < 0.14$ the system is better described as a mixture of $F4/mmm$-type structures, with interstitial oxygen defects, and an almost stoichiometric ($\delta = 0.00(2)$) $Bmab$-type phase. This phase boundary is difficult to establish. In principle it may even depend on the sample preparation procedure. Jorgensen *et al* [10] propose the phase boundary at $\delta = 0.02$. However, if we use data from [14] and [26] we are able to push the phase boundary for the high-temperature phase transition as well as for the magnetic transition until $\delta \simeq 0.09$. Data of [14] and [26] are from single crystals, where it is more difficult to control the homogeneity of the oxygen stoichiometry and detect the phase mixture. In our case we are able to define a point in the mixed phase region of the phase diagram. Our sample was composed of $F4/mmm$ phase ($\delta = 0.10$) and $Bmab$ ($\delta < 0.01$), giving an overall oxygen content of $\delta \simeq 0.07$. In order to fit the magnetic reflections of our data at 1.5 K, we have to allow some Ni^{2+} ordered moment in the $F4/mmm$ phase. A complete phase diagram, however, in the mixed phase region is not available with the present data.

In the oxygen-rich side a single average phase $F4/mmm$ is present with a high concentration of oxygen defects. The phase boundary will probably be around $\delta \simeq 0.14$.

The low-temperature structural phase transition is only characterized for two overall oxygen concentrations, $\delta \simeq 0$ and $\delta \simeq 0.07$, but the phase boundary to higher oxygen content is not known. The T_1 point for the mixed phase ($\delta \simeq 0.07$) corresponds to the overall excess oxygen concentration of our sample. However, we know that the only phase which undergoes the low-temperature structural phase transition is the almost stoichiometric $\delta < 0.02$ *Bmab* phase. Indeed, because this phase transition is related to the tilt of oxygens in the Ni^{2+} octahedra, an oxygen excess of $\delta > 0.02$ may preclude the transition.

4. Conclusions

The sensitivity of the different structural phase transitions to the hole doping (we shall restrict the discussion to the case of hole doping via oxygen excess) can be explained qualitatively by a very simple model that takes into account only crystal chemical considerations. The instabilities of the structure of the Ln_2NiO_4 oxides can be related to the mismatch between the Ln_2O_2 layers with the NaCl structure and the perovskite layers NiO_2, and to the different thermal expansion coefficients of the two types of layers [27]. At high temperatures, in air atmosphere, perfect matching between the two layers is achieved by incorporating interstitial oxygens in the Ln_2O_2 layers from the environment. The excess oxygen prevents the rotation of the NiO_6 octahedra and the $F4/mmm$ is stabilized in a large temperature range. It can be expected that, on lowering the ionic radius of the Ln (going from La to Nd), the amount of excess oxygen must increase for the same conditions of oxygen pressure and temperature. In reducing the samples up to perfect stoichiometry, a rise of T_0 and T_1 must be expected, in agreement with the experimental results for Pr and Nd (see [5, 6]). All these structural phase transitions do not require any electronic band instability to be explained; however, the occurrence of these transitions may play a role in the electronic properties of these materials. A study by computer simulation is under way with the goal of exploring and proving more precisely the above statements.

The last point to be commented upon is the similarities and differences between the rare-earth superconducting cuprates and non-superconducting nickelates. In comparison with the hole superconductors (La_2CuO_4 type), the rare-earth nickelates present similar structure and magnetic properties. The main difference, from the structural point of view, is in the metal octahedron. In the case of La_2CuO_4 type, this octahedron is very much elongated (distorted); for instance the ratio $Cu-O1/Cu-O2 = 1.907$ Å$/2.459$ Å $\simeq 0.77$ [28]. In contrast, for the nickelates, $Ni-O1/Ni-O2 = 1.944$ Å$/2.235$ Å $\simeq 0.87$.

From the magnetic point of view the difference, beside the spin $\frac{1}{2}$ for Cu or 1 for Ni, is in the magnetic structure. La_2CuO_4 orders in a $\Gamma_{4g}(-++)$, i.e. $g_y a_z$ mode. Below the Néel temperature, there thus exists the possibility of an AF component along the c axis, and the main component of the magnetic moment points along the b axis. In contrast, the nickelates order in a pure g_x mode. The magnetic moments point along the octahedra tilt axis ([100]). In the case of La_2NiO_4 below T_1, there is the possibility of a ferromagnetic component along the c axis. The difference between both types of magnetic ordering for La_2CuO_4-type or Ni-based compounds could probably be related with the single-ion anisotropy and/or Dzyaloshinsky–Moriya antisymmetric exchange interactions, which could be very different between La_2CuO_4 and nickelates. A study of the

stability of the different magnetic structures as a function of the isotropic and anisotropic exchange parameters will be published elsewhere in the future.

The introduction of interstitial oxygens has a strong influence on the magnetic properties owing to effective hole doping. The oxidized sample does not order, at least for temperatures higher than 1.5 K. The partially oxidized sample shows an AF ordering, with T_N lower than in the case of the stoichiometric counterpart. The mechanism of how the oxygen excess breaks the long-range magnetic ordering is not yet clearly established. However, a plausible explanation could be the following. Holes in the NiO$_2$ plane produce ferromagnetic (Ni^{2+}–O$^-$–Ni^{2+}) interactions between nearest neighbours, which are in competition with the normal antiferromagnetic superexchange (Ni^{2+}–O^{2-}–Ni^{2+}) interaction. The resulting frustration will preclude the 3D long-range AF ordering.

The stoichiometric compounds are insulators. Doping with oxygen makes the system metallic at temperatures above 400 K, and in the case of the cuprates hole superconductors at low temperature. Which properties preclude the nickelates to become superconductors are not clear to us. However, any theoretical explanation of the superconductivity in copper oxides should give a reason for this difference between nickelates and La$_2$CuO$_4$.

Acknowledgments

Appendix. Anisotropic broadening of Bragg reflections and Rietveld method

Strains in real materials induce broadening of Bragg reflections. An elementary way to understand this effect is to consider that the presence of microstrains is equivalent to the existence of a distribution of cell parameters within a sample. Well defined values of the cell parameters produce sharp peaks in a diffraction pattern, whereas a distribution of cell parameters produces broadening of the peaks.

The origin of microstrains can be variable. For example, the presence of random vacancies in a cubic lattice gives rise to spatial fluctuations of the cell constants. The assumed randomness induces isotropic broadening of reflections. If the mean fluctuation is Δa, the angular spread of the intensity is given by $\Delta(2\theta) = 2(\Delta a/a)\tan\theta$, where $\Delta a/a$ is independent of $(h\,k\,l)$.

Let us assume a Gaussian distribution of a particular cell parameter x, of mean value α and variance $\sigma^2(\alpha)$. The probability of finding the value x is given by the normal distribution:

$$P(x) = \frac{1}{\sigma(\alpha)}(2\pi)^{1/2}\exp\left(-\frac{1}{2}\frac{(x-\alpha)^2}{\sigma^2(\alpha)}\right). \tag{A1}$$

The full width at half-maximum (FWHM) is related to the variance by:

$$\text{FWHM} = 2(2\ln 2)^{1/2}\sigma(\alpha).$$

The relevant variable for diffraction patterns is the squared inverse of the lattice spacing, which is a function of the cell parameters and the Miller indices:

$$M_{hkl} = 1/d_{hkl}^2 = M(\alpha_i; hkl) \tag{A2}$$

where α_i ($i = 1, 2, \ldots, 6$) are direct or reciprocal cell parameters, or, in general, any set

of six parameters defining the metric of the unit cell. The α_i parameters are considered as normally distributed random variables of mean values $\langle \alpha_i \rangle$, with a covariance matrix of components $S_{ij} = \mathrm{cov}(\alpha_i \alpha_j)$ $[\mathrm{cov}(\alpha_i \alpha_i) = \sigma^2(\alpha_i)]$; the mean value of M and its variance are given by:

$$\langle M_{hkl} \rangle = M(\langle \alpha_i \rangle; hkl) \tag{A3}$$

$$\sigma^2(M_{hkl}) = \sum_i \sum_j S_{ij} \frac{\partial M}{\partial \alpha_i} \frac{\partial M}{\partial \alpha_j}. \tag{A4}$$

One can assume that the peak broadening due to the cell parameter fluctuations and correlations, defined by the covariance matrix S_{ij}, is of Gaussian character. Therefore the square of the broadening produced by the strains must be added to the square of the instrumental broadening to obtain the square of the observed width of the peaks.

From the Bragg law one can obtain the relation between the variance of the peak profile, due to microstrains, and the variance of M_{hkl}:

$$\sigma^2(2\theta)_s = [\sigma^2(M_{hkl})/M_{hkl}^2]\tan^2\theta \tag{A5}$$

or, in terms of the halfwidth:

$$\mathrm{FWHM}^2(2\theta)_s = (8\ln 2)\sigma^2(2\theta)_s.$$

In Rietveld refinements, the halfwidth parameters U, V and W characterize the instrumental resolution curve. Assuming a Gaussian instrumental peak shape, the resolution curve is given by the Cagliotti expression:

$$\mathrm{FWHM}^2(2\theta)_{\mathrm{ins}} = U\tan^2\theta + V\tan\theta + W. \tag{A6}$$

The modified expression taking into account the presence of microstrains is

$$\mathrm{FWHM}^2(2\theta) = \{U + (8\ln 2)[\sigma^2(M_{hkl})/M_{hkl}^2]\}\tan^2\theta + V\tan\theta + W. \tag{A7}$$

The above formalism is just a simple way to write down expressions relating the broadening of reflections as a function of hkl. It is useful only when microstrains can be reduced to some kind of generalized cell parameter fluctuations and correlations. The modelling of a particular pattern of microstrains is equivalent to constructing a particular covariance matrix, which must be obtained from the analysis of the peak broadening. In some cases, the microstrains can be related via the elastic constants with the microstress existing in the sample. However, the macroscopic character of the elastic constants makes a physical interpretation of the stress difficult.

Using the formalism presented above, we have been able to find a very simple model that allows the refinement of the powder neutron diffraction profile corresponding to the LTT phase of stoichiometric La_2NiO_4. Considering an average tetragonal lattice with locally correlated orthorhombic distortions, as we have discussed in the text, the following parameters have to be taken in order to calculate the peak broadening:

$$\langle a \rangle = \langle b \rangle = a_T \qquad \langle c \rangle = c_T \qquad \sigma^2(a) = \sigma^2(b) = \sigma^2 \qquad \sigma^2(c) = 0$$

$$\mathrm{cov}(a, b) = -\sigma^2 \qquad \Leftrightarrow \qquad \mathrm{corr}(a, b) = \mathrm{cov}(a, b)/\sigma(a)\sigma(b) = -1.$$

Using the formula (A4) and defining the microstrain parameter as $\varepsilon = \sigma/a_T$ one obtains

$$\sigma^2(M_{hkl}) = 4(h^2 - k^2)^2\sigma^2/a_T^6 = 4(h^2 - k^2)^2\varepsilon^2/a_T^4. \tag{A8}$$

The FWHM$_s$ of the reflections is given by the formula:

$$\mathrm{FWHM}(2\theta)_s = \frac{4(2\ln 2)^{1/2}|h^2 - k^2|\varepsilon}{a_T^2[(h^2 + k^2)/a_T^2 + l^2/c_T^2]} \tan\theta. \tag{A9}$$

From this expression it is clear that the reflections of type $(h\,h\,l)$ are sharp, while those with $h \neq k$ are strongly broadened. The introduction of an extra parameter in the refinement as explained above allows a much more satisfactory fit of the experimental data (figure 2(b)).

In the case of the oxidized sample (O) the existence of interstitial oxygens give rise to microstrains. The oxygen excess concentration in our sample corresponds roughly to six oxygens more per ten unit cells of the $F4/mmm$ space group. The induced microstrain is very small and, if we assume that the main fluctuations of the cell parameters take place in the ab plane, whatever model of strain improves the refinement. The value of the microstrain parameter given in table 2 corresponds to the model described by the formula (A9).

References

[1] Rodríguez-Carvajal J, Martínez J L, Pannetier J and Saez-Puche R 1988 *Phys. Rev.* B **38** 7148
    Saez-Puche R, Fernández F, Martínez J L and Rodríguez-Carvajal J 1989 *J. Less Common Met.* **149** 357
[2] Axe J D, Cox D E, Mohanty K, Moudden H, Moodenbaugh A R, Youwen Xu and Thurston T R 1989 *IBM J. Res. Dev.* **33** 382
[3] Axe J D, Moudden H, Hohlwein D, Cox D E, Mohanty K M, Moodenbaugh A R and Youwen Xu 1989 *Phys. Rev. Lett.* **62** 2751
[4] Lander G H, Brown P J, Honig J M and Spalek J 1989 *Phys. Rev.* B **40** 4463
[5] Rodríguez-Carvajal J, Fernández-Díaz M T, Martínez J L, Fernández F and Saez-Puche R 1990 *Europhys. Lett.* **11** 261
[6] Fernández-Díaz M T, Rodríguez-Carvajal J, Martínez J L, Fillion G, Fernández F and Saez-Puche R 1991 *Z. Phys.* B **82** 275
[7] Kakol Z, Spalek J and Honig J M 1989 *J. Solid State Chem.* **79** 288; 1989 *Solid State Commun.* **71** 283
    Spalek J, Kakol Z and Honig J M 1989 *Solid State Commun.* **71** 511
[8] Buttrey D J, Ganguly P, Honig J M, Rao C N R, Schartman R R and Subbanna G N 1988 *J. Solid State Chem.* **74** 233
[9] Bishop A R, Martin R L, Müller K A and Tesanovic Z 1989 *Z. Phys.* B **76** 17
[10] Jorgensen J D, Dabrowski B, Shiyou Pei, Richards D R and Hinks D G 1989 *Phys. Rev.* B **40** 2187
[11] Ganguly P 1986 *Advances in Solid State Chemistry* ed C N R Rao (New Delhi: Indian National Science Academy) p 135
[12] Choisnet J, Bassat J M, Pilliere H, Odier P and Leblanc M 1989 *Solid State Commun.* **66** 1245
[13] Battle X, García-Muñoz J L, Medarde M, Rodríguez-Carvajal J, Obradors X, Martínez J L, Vallet M, Gonzalez-Calbet J, Sayagués M J and Fontcuberta J 1989 *Physica* C **162–164** 1273
[14] Aeppli G and Buttrey D J 1988 *Phys. Rev. Lett.* **61** 203 and private communication
[15] Saez-Puche R, Rodríguez J L and Fernández F 1987 *Inorg. Chim. Acta* **140** 151
[16] Rodríguez-Carvajal J, Anne M and Pannetier J 1987 *Institut Laue-Langevin Report* No 87Ro14T unpublished
[17] Rodríguez-Carvajal J 1990 *Abstracts of Satellite Meeting on Powder Diffraction of XVth Congr. Int. Union of Crystallography (Toulouse, 1990)* p 127
[18] Petzelt J 1975 *J. Phys. Chem. Solids* **36** 1005
    Arend H, Hofmann R and Waldner F 1973 *Solid State Commun.* **11** 1629

[19] Alexandrov K S 1987 *Kristallografiya* **32** 937; (*Sov. Phys.–Crystallogr.* **32** 551)
    Alexandrov K, Beznosikov B V and Misyul S V 1987 *Phys. Status Solidi* A **104** 529
    Hatch D M, Stokes H T, Alexandrov K S and Misyul S V 1989 *Phys. Rev.* B **39** 9282
[20] Chaillout C, Cheong S W, Fisk Z, Lehmann M S, Marezio M, Morosin B and Schirber J E 1989 *Physica*
    C **158** 183
[21] Kajitani T, Hirabayashi M, Fukuda T and Onozuka T 1989 *J. Phys. Soc. Japan* **58** 3616
[22] Krishnan R S, Srinivasan R and Devanorayanan S 1979 *Thermal Expansion of Crystals* (Oxford:
    Pergamon)
[23] Fernández F, Saez-Puche R, Fernández-Díaz M T, Rodríguez-Carvajal J, Martínez J L, Botto I L and
    Baran E J 1991 *Eur. J. Solid State Inorg. Chem.* **28** 507
[24] Brown P J 1988 *Institut Laue–Langevin Report* SP88BR5026 unpublished
[25] Bertaut E F 1968 *Ann. Phys.* A **24** 217
[26] Buttrey D J, Honig J M and Rao C N R 1986 *J. Solid State Chem.* **64** 287
[27] Manthiram A, Tang X and Goodenough J B 1990 *Phys. Rev.* B **42** 138
    Kransin'kova M V and Moizhes B Ya 1990 *Sov. Phys.–Solid State* **32** 184
[28] Wilson J A 1988 *J. Phys. C: Solid State Phys.* **21** 2067